

Anisotropy and nonlinearity in superlattices II

M. F. Pereira¹ 

Received: 5 May 2016 / Accepted: 13 July 2016 / Published online: 10 August 2016
© The Author(s) 2016. This article is published with open access at Springerlink.com

Abstract This paper uses the anisotropic medium approach to calculate nonlinear optical absorption in semiconductor superlattices. The study confirms that the nonlinearities increase with anisotropy suggesting that strongly anisotropic materials such as those used for solar cells may also play a relevant role for nonlinear optical applications.

Keywords Semiconductor superlattices · Anisotropic medium approach · Many body effects

1 Introduction

Superlattices offer possibilities to study transport (Wacker 2002) and optical (Pereira 1995) properties of semiconductor under controlled conditions. This paper uses the anisotropic medium approach that can be easily programmed and includes the main many body effects required to describe steady state nonlinear absorption. The expressions delivered reduce exactly to Elliott's formula in the low density linear limit. This leads to an efficient numerical tool to investigate new materials, starting e.g. from ab initio calculations. This has potential for a major impact in the development of new materials with applications from terahertz (THz) and mid-infrared (MIR) to the visible (VIS) spectral range (Pereira 2015). The superlattices are modelled as anisotropic media characterized by effective masses parallel and perpendicular to the growth direction (Pereira 1995). That suggests that

This article is part of the Topical Collection on Advances in the Science of Light.

Guest Edited by Jelena Radovanovic, Milutin Stepic, Mikhail Sumetsky, Mauro Pereira and Dragan Indjin.

✉ M. F. Pereira
m.pereira@shu.ac.uk

¹ Materials and Engineering Research Institute, Sheffield Hallam University, S1 1WB Sheffield, UK

new materials being currently investigated for solar cells and which are strongly anisotropic (Steinmann et al. 2015), may also be very useful for nonlinear optics applications, e.g. the controllable anisotropy in the superlattice case might be useful for applications such as power limiting (Poirier et al. 2002; Wu et al. 2003). Here the anisotropy-induced nonlinearity in the nanostructure is controlled per design in contrast with less controllable recent studies in which it depends on the nanoparticle shape (Hua et al. 2015). We show that the nonlinearities increase with the anisotropic character, but the results are only valid as long as sufficient tunnelling occurs. In other words, isolated quantum wells should not be addressed by this method. This paper extends and complements the study in Pereira (2016) with different well widths and a more detailed analysis of the population inversion and is organized as follows: first, the main equations used are summarized. Next, numerical applications for GaAs/AlGaAs superlattices are given and a short summary follows.

2 Mathematical approach and model equations

The carrier-induced optical nonlinearities of semiconductors can be obtained by the self-consistent evaluation of Many Body Nonequilibrium Green's Functions (NEGF). Efficient numerical methods used here have been successfully applied to both inter-subband (Pereira and Faragai 2014; Pereira 2007, 2008, 2011; Pereira et al. 2007; Pereira and Tomić 2011) and inter-band transitions (Gempel et al. 1996; Pereira et al. 1994; Pereira and Henneberger 1997; Chow et al. 1992) in quantum wells and superlattices. For completeness, we repeat here the main equations of Pereira (2016) for a guide to the reader, by starting with the interband polarization that has been used to describe superlattices as an effective anisotropic 3D material (Pereira 1995),

$$\left[\hbar\omega + i\Gamma - E_g(\gamma) - \frac{\hbar^2 k^2}{2\mu_{\parallel}} \xi(\theta, \gamma) \right] P(\vec{k}, \omega) = A(\omega) \left[\varphi \cdot E(\omega) + \sum_{\vec{k}' \neq \vec{k}} \mathcal{W}_{\vec{k}-\vec{k}'} P(\vec{k}', \omega) \right], \quad (1)$$

where the meaning of the anisotropy dependent bandgap is explained below and $\xi(\theta, \gamma) = \sin^2\theta + \gamma\cos^2\theta$. The anisotropy parameter γ is given by the ratio between the in-plane μ_{\parallel} and perpendicular μ_{\perp} reduced effective masses, $\gamma = \mu_{\parallel}/\mu_{\perp}$, with $\frac{1}{\mu_{\parallel}} = \frac{1}{m_{e\parallel}} + \frac{1}{m_{h\parallel}}$ and $\frac{1}{\mu_{\perp}} = \frac{1}{m_{e\perp}} + \frac{1}{m_{h\perp}}$ which are calculated from the non-interacting superlattice Hamiltonian \mathcal{H}_0 , $\frac{1}{m_{i\parallel}} = \hbar^{-2} \partial^2 / \partial k_{i\parallel}^2 \Psi | \mathcal{H}_0 | \Psi$, $\frac{1}{m_{i\perp}} = \hbar^{-2} \partial^2 / \partial k_{i\perp}^2 \Psi | \mathcal{H}_0 | \Psi$, for $i = e, h$. More details are given in Pereira (1995). A phenomenological scattering rate Γ is used to simulate the average dephasing that stems from the electron–electron, electron–phonon and electron–impurity scattering (Chow et al. 1992; Schmielau and Pereira 2009a, b), in order to keep the approach as simple as possible without affecting the conclusions. We have neglected any k -dependence on the transition dipole moment φ induced by the electric field $E(\omega)$. In a superlattices there is a preferred direction determined by the growth (z-direction), leading to cylindrical symmetry. The next step is to perform an angle average, $\langle \xi(\theta, \gamma) \rangle = \langle \sin^2\theta + \gamma\cos^2\theta \rangle = \frac{1}{2}(1 + \gamma)$ and thus

$$\frac{\hbar^2 k^2}{2\mu_{\parallel}} \xi(\theta, \gamma) \rightarrow \frac{\hbar^2 k^2}{2M_{\parallel}}. \quad (2)$$

The resulting anisotropic mass $M_{\parallel} = 2\mu_{\parallel}/(1 + \gamma)$ determines the exciton Bohr radius a_0 and corresponding 1S binding energy E_0 ,

$$a_0 = a_0(\gamma) = \hbar^2 \epsilon_0 / e^2 M_{\parallel}, \quad E_0 = E_0(\gamma) = 2Ry / (1 + \gamma), \quad Ry = \frac{\mu_{\parallel} e^4}{2\hbar^2 \epsilon_0^2}, \quad (3)$$

where ϵ_0 and e denote, respectively the background dielectric constant and the electron charge. The resulting exciton binding energies in superlattices are in very good agreement with experiments, as demonstrated in Pereira (1995).

By approximating the full inversion factor by $A(\omega) = \tanh[\beta(\hbar\omega - \mu)/2]$ we make sure that the cross-over from absorption to gain takes place exactly at the total chemical potential. Next, we replace the usual Yukawa potential describing screened carriers in 3D (which does not have analytical solutions for the corresponding Schrödinger equation) by the Hulthén potential $\mathcal{W}(r) = -2e^2 \kappa \epsilon_0^{-1} / (\exp(2\kappa r) - 1)$ (Pereira 1995; Bányai and Koch 1986; Flügge 1974), which has successfully reproduced bulk nonlinear optical spectra (Schmielau and Pereira 2009c) and has well known analytical solutions.

The total chemical potential $\mu = \mu_e + \mu_h$ and screening wavelength $\kappa = \kappa_e + \kappa_h$ are given by

$$\beta\mu_{\lambda} = \ln v_{\lambda} + K_1 \ln(K_2 v_{\lambda} + 1) + K_3 \mu_{\lambda}, \quad (4)$$

$$\kappa_{\lambda} = \sqrt{\frac{4\pi e^2}{\epsilon_0} \frac{\partial n_{\lambda}}{\partial \mu_{\lambda}}} = \sqrt{\frac{\beta \pi e^2 n_{\lambda} / \epsilon_0}{\frac{1}{v_{\lambda}} + \frac{K_1 K_2}{K_2 v_{\lambda} + 1} + K_3}}, \quad (5)$$

where $K_1 = 4.897$, $K_2 = 0.045$ and $K_3 = 0.133$. The parameter v_{λ} is obtained from the particle density for electrons and holes, $n = n_e = n_h$ by $v_{\lambda} = 4n_{\lambda} / [(2m_{\parallel,\lambda} / \beta \pi \hbar^2)(2m_{\perp,\lambda} / \beta \pi \hbar^2)^{1/2}]$ and $\beta = 1/K_B T$ (Pereira 1995).

It is beyond the scope of this paper to show the intermediate details that lead Eq. (6). The main steps are to combine the partly phenomenological approach of Bányai and Koch (1986) with the material parameters calculated with the anisotropic medium approach (Pereira 1995; Pereira et al. 1990). Furthermore, we use hypergeometric functions instead of the Jost function approach of Pereira (1995) and Flügge (1974). The resulting absorption spectrum then reads

$$\alpha(\omega) = \alpha_0(\gamma) \frac{\hbar\omega}{e_0} \tanh[\beta(\hbar\omega - \mu)/2] \left\{ \sum_{n=1}^{\sqrt{g}} \frac{4\pi}{n} \left(\frac{1}{n^2} - \frac{n^2}{g^2} \right) \delta_{\Gamma}(\Delta - e_n) + 2\pi \int_0^{\infty} \frac{\sinh(\pi g \sqrt{x})}{\cosh(\pi g \sqrt{x}) - \cos(\sqrt{4g - g^2 x})} \delta_{\Gamma}(\Delta(-x)) dx \right\}, \quad (6)$$

where $\alpha_0(\gamma) = 2\phi^2 / (n_b \hbar c a_0^3(\gamma))$. The normalized detuning is $\Delta = (\hbar\omega - E_g(\gamma)) - E_0(\gamma)$. Here, and c denote, respectively, the background refractive index and the speed of light in vacuum. In Eq. (6) above, the band gap renormalization stems from the Mott criterion. This expression for the bandgap renormalization is usually in good agreement with the full Green's function approach and the Single Plasmon Pole Approximation (SPPA) simplified under a quasi-static approximation (Pereira 1995).

$$E_g(\gamma) = E_{gap} + E_0(\gamma) \begin{cases} -1 + \left(1 - \frac{1}{g(\gamma)}\right)^2, & g(\gamma) \geq 1 \\ -1/g(\gamma), & g(\gamma) < 1 \end{cases} \quad (7)$$

where $g(\gamma) = 1/\kappa a_0(\gamma)$ and $E_{gap} = E_c(1) + E_{HH}(1) + E_{gap,bulk}$ is the bulk (temperature dependent) isotropic bandgap found in semiconductor material tables in the literature plus the confinement energies of the lowest conduction subband and the top heavy hole subband.

The broadened delta function representation is $\delta_\Gamma(x) = 1/\pi\delta\eta\cosh(x/\eta)$, where $\eta = \Gamma/E_0(\gamma)$ which reproduces the Urbach tail very efficiently. The sum in the exciton part runs through the available states within the largest integer value of $\sqrt{g(\gamma)}$. In the low density limit, $g(\gamma) \rightarrow \infty$ and we recover the Elliot formula for excitonic luminescence with the correct balance between bound and continuum states.

3 Numerical results and discussion

Figure 1 depicts the nonlinear optical absorption of GaAs–Al_{0.3}Ga_{0.7}As superlattices at $T = 300$ K. The scaled photon energy (x -axis) highlights the Coulomb correction effects that would otherwise be mixed with the changes due to carrier confinement by increasing the well width, included in $E_{gap} = E_c(1) + E_{HH}(1) + E_{gap,bulk}$.

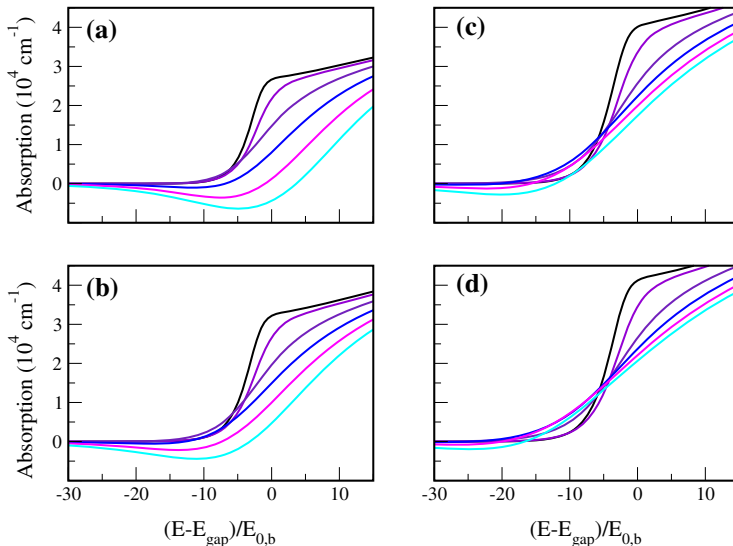


Fig. 1 Nonlinear optical absorption of GaAs–Al_{0.3}Ga_{0.7}As superlattices at 300 K with increasing anisotropy characterized by decreasing $\gamma = 0.61, 0.42, 0.20$ and 0.11 , respectively from **a–d**. This is obtained by fixing the barrier width at 6 nm and increasing the well width correspondingly by 1, 2, 4 and 6 nm. In each panel, from top to bottom the carrier density in both conduction and valence bands is $N = 0, 0.1, 0.5, 1, 1.5$ and $2 \times 10^{18} \text{ cm}^{-3}$. $E_{0,b} = 4.2 \text{ meV}$ is the bulk GaAs exciton binding energy. From **a–d**, $E_{gap} = 2.092, 2.0135, 1.918, 1.873 \text{ eV}$

The increase in anisotropy (smaller γ) by increasing the quantum well length, stems from reducing the wavefunction overlap through the barrier, here measured by a larger mass along the growth direction. The single quantum well case would be obtained for a very large barrier, with $\mu_{\perp} \rightarrow \infty$ and correspondingly $\gamma \rightarrow 0$. However, this method should not be used in the quasi-2D case and calculations dedicated to quantum wells (see e.g. Pereira et al. 1994) should be used. From (a) to (d) we do see an increase in nonlinearity, i.e. a larger reduction in absorption with increasing carrier density. Note that even though Pereira (1995) also has analytical expressions for the nonlinear spectra of superlattices, to the best of that author's knowledge numerical applications have never been given before as in the present paper. Figure 2 makes it more clear by showing the differential absorption $\Delta\alpha(\omega) = \alpha(\omega, N) - \alpha(\omega, N = 0)$.

Figure 3 allows a better understanding of the excitonic bleaching and gain development as a function of anisotropy and carrier density.

The combined figures show that as the anisotropy increases (smaller γ , so does the inverse screening length κ leading to a faster reduction of the screened Coulomb interaction and consequently larger optical nonlinearity, measured here directly by the differential absorption. This shows that an increase in nonlinearity is observed for all carrier densities, which are considered in the manuscript, and in the whole range of energies depicted in Fig. 1. Note however that it only makes sense to consider the range of linear to saturated absorption in the differential transmission calculations while two positive values are compared. The negative absorption (gain) confuses the comparison.

By increasing the anisotropy, the z-direction electron and hole masses become too different, with a much larger increase in hole mass. When the upper and lower (average) curvatures or equivalently, the average effective masses are too different the total chemical potential is relatively smaller (see Fig. 3b) and so is the inversion factor $A(\omega) = \tanh[\beta(\hbar\omega - \mu)/2]$ of Eqs. (1) and (6), thus reducing the gain in Fig. 1. This influence of different electron and hole masses on the inversion/gain is fully consistent with the detailed analysis for isolated quantum wells seen e.g. in Pereira and Henneberger (1997). The results are complemented by a two-dimensional plot of the population inversion factor as a function of detuning and anisotropy parameter in Fig. 4.

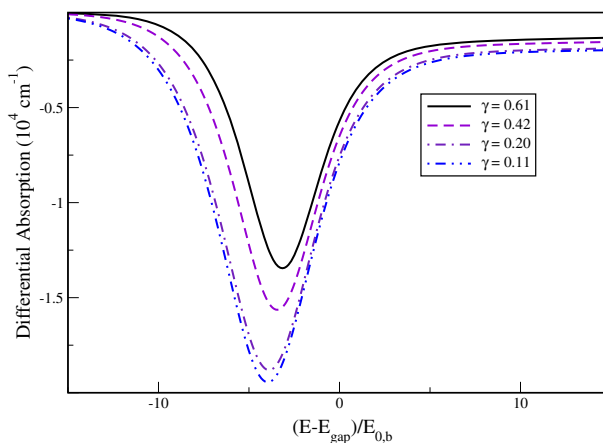


Fig. 2 Differential absorption $\Delta\alpha(\omega) = \alpha(\omega, N) - \alpha(\omega, N = 0)$ for the structures in Fig. 1 with a carrier density $N = 1 \times 10^{17} \text{ cm}^{-3}$ at 300 K. The solid, dashed, dot-dashed and dot-double dashed correspond to an increase in anisotropy, characterized respectively by $\gamma = 0.61, 0.42, 0.20$ and 0.11

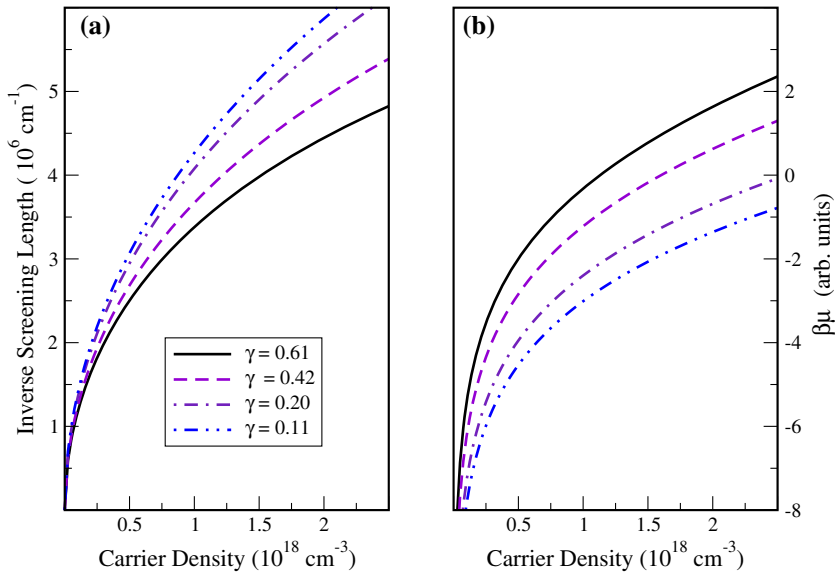


Fig. 3 Inverse screening length κ (a) and total chemical potential $\beta\mu$ (b) as a function of carrier density for the same structures in Figs. 1 and 2 at 300 K. The *solid*, *dashed*, *dot-dashed* and *dot-double dashed* correspond to an increase in anisotropy, characterized respectively by $\gamma = 0.61, 0.42, 0.20$ and 0.11

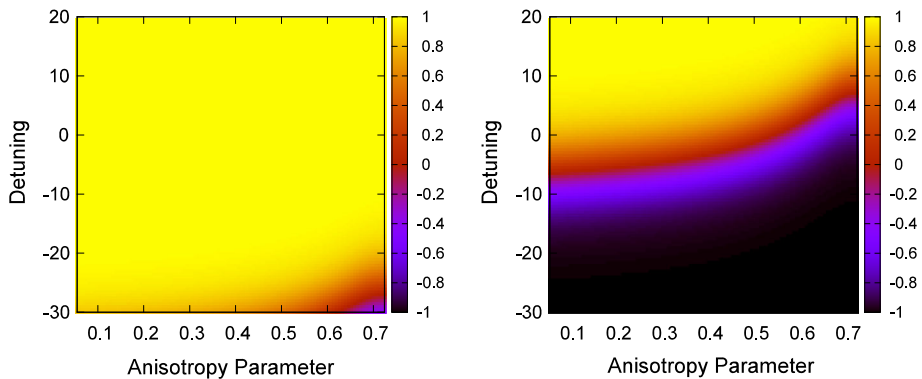


Fig. 4 Population inversion factor $A(\omega)$ of Eq. (1) as a function of detuning and anisotropy parameter at 300 K. The *left* and *right panels* are respectively for population densities $N = 0.02$ and $2 \times 10^{18} \text{ cm}^{-3}$

Note the larger inversion region and values (the factor gets more negative) for smaller anisotropy (larger γ). The method used here can be used for a variety of other materials and superlattices as long as tunnelling between adjacent periods allows a 3D-like spread of carriers wavefunctions—either electrons or holes so that movement along the z -direction is possible and an effective 3D medium can be considered with corresponding effective masses. Thus the model is better suited for absorption in superlattices far from the 2D limit. In the quasi-2D limit of quantum wells, the full numerical solution (Grepel et al. 1996; Pereira et al. 1994; Pereira and Henneberger 1997) should be used. Thus, increase in nonlinearity is clearly demonstrated, which may be very important for truly 3D anisotropic

new materials, but the high gain in quantum wells cannot be described by the method presented here.

In summary, the analytical expressions developed confirm the connection between an increase in optical nonlinearity with anisotropy by directly controlling the anisotropy and evaluating the resulting differential absorption and nonlinear spectra. This study illustrates the potential for three dimensional strongly anisotropic semiconductor materials for a role in nonlinear optics and a possible recipe to improve their efficiency by controlling the anisotropy.

Acknowledgments The author acknowledges support from MPNS COST ACTION MP1204—TERA-MIR Radiation: Materials, Generation, Detection and Applications and BM1205 European Network for Skin Cancer Detection using Laser Imaging.

Open Access This article is distributed under the terms of the Creative Commons Attribution 4.0 International License (<http://creativecommons.org/licenses/by/4.0/>), which permits unrestricted use, distribution, and reproduction in any medium, provided you give appropriate credit to the original author(s) and the source, provide a link to the Creative Commons license, and indicate if changes were made.

References

- Bányai, L., Koch, S.W.: A simple theory for the effects of plasma screening on the optical spectra of highly excited semiconductors. *Z. Phys. B* **63**, 283–291 (1986)
- Chow, W.W., Pereira Jr., M.F., Koch, S.W.: Many-body treatment on the modulation response in a strained quantum well semiconductor laser medium. *Appl. Phys. Lett.* **61**, 758–760 (1992)
- Flügge, S.: *Practical Quantum Mechanics*. Springer, New York (1974)
- Grempe, H., Diessel, A., Ebeling, W., Gutowski, J., Schuell, K., Jobst, B., Pereira Jr., M.F., Henneberger, K.: High-density effects, stimulated emission and electrooptical properties of ZnCdSe/ZnSe single quantum wells and laser diodes. *Phys. Status Solidi B* **194**, 199–217 (1996)
- Hua, Y., Chandra, K., Dam, D.H., Wiederrecht, G.P., Odom, T.W.: Shape-dependent nonlinear optical properties of anisotropic gold nanoparticles. *J. Phys. Chem. Lett.* **6**, 4904–4908 (2015)
- Pereira Jr., M.F.: Analytical solutions for the optical absorption of superlattices. *Phys. Rev. B* **52**, 1978–1983 (1995)
- Pereira Jr., M.E.: Intersubband antipolaritons: microscopic approach. *Phys. Rev. B* **75**, 195301-1–195301-5 (2007)
- Pereira Jr., M.E.: Intervalence electric mode terahertz lasing without population inversion. *Phys. Rev. B* **78**, 245305-1–245305-5 (2008)
- Pereira Jr., M.F.: Microscopic approach for intersubband-based thermophotovoltaic structures in the THz and mid infrared. *JOSA B* **28**, 2014–2017 (2011)
- Pereira, M.F.: TERA-MIR radiation: materials, generation, detection and applications II. *Opt. Quantum Electron.* **47**, 815–820 (2015)
- Pereira, M.F.: Anisotropy and nonlinearity in superlattices. *Opt. Quant. Electron.* **48**(6), 321-1–321-7 (2016)
- Pereira, M.F., Faragai, I.A.: Coupling of THz radiation with intervalence band transitions in microcavities. *Opt. Express* **22**, 3439–3446 (2014)
- Pereira Jr., M.F., Henneberger, K.: Gain mechanisms and lasing in II–VI compounds. *Phys. Status Solidi B* **202**, 751–762 (1997)
- Pereira, M.F., Tomić, S.: Intersubband gain without global inversion through dilute nitride band engineering. *Appl. Phys. Lett.* **98**, 061101-1–061101-3 (2011)
- Pereira Jr., M.F., Galbraith, I., Koch, S.W., Duggan, G.: Exciton binding energies in semiconductor superlattices: an anisotropic effective-medium approach. *Phys. Rev. B* **42**, 7084–7089 (1990)
- Pereira Jr., M.F., Binder, R., Koch, S.W.: Theory of nonlinear absorption in coupled band quantum wells with many-body effects. *Appl. Phys. Lett.* **64**, 279–281 (1994)
- Pereira Jr., M.F., Nelander, R., Wacker, A., Revin, D.G., Soulby, M.R., Wilson, L.R., Cockburn, J.W., Krysa, A.B., Roberts, J.S., Airey, R.J.: Characterization of intersubband devices combining a nonequilibrium many body theory with transmission spectroscopy experiments. *J. Mater. Sci. Mater. Electron.* **18**, 689–694 (2007)

- Poirier, G., de Araújo, C.B., Messaddeq, Y., Ribeiro, S.J.L., Poulain, M.: Tungstate fluorophosphate glasses as optical limiters. *J. Appl. Phys.* **91**, 10221–10223 (2002)
- Schmielau, T., Pereira Jr., M.F.: Nonequilibrium many body theory for quantum transport in terahertz quantum cascade lasers. *Appl. Phys. Lett.* **95**, 231111-1–231111-3 (2009a)
- Schmielau, T., Pereira, M.F.: Impact of momentum dependent matrix elements on scattering effects in quantum cascade lasers. *Phys. Status Solidi B* **246**, 329–331 (2009b)
- Schmielau, T., Pereira, M.F.: Momentum Dependent Scattering Matrix Elements in Quantum Cascade Laser Transport. *Microelectron. J.* **40**, 869–871 (2009c)
- Steinmann, V., Brandt, R.E., Buonassisi, T.: Photovoltaics: non-cubic solar cell materials. *Nat. Photonics* **9**, 355–357 (2015)
- Wacker, A.: Semiconductor superlattices: a model system for nonlinear transport. *Phys. Rep.* **357**, 1–111 (2002)
- Wu, P., Philip, R., Laghumavarapu, R.B., Devulapalli, J., Rao, D.V.G.L.N., Kimball, B.R., Nakashima, M., DeCristofano, B.S.: Optical power limiting with photoinduced anisotropy of azobenzene films. *Appl. Opt.* **42**, 4560–4565 (2003)